Nordic Hydrology, 15, 1984, 131-144

Effect of Local Bottom Slope and Roughness Coefficient Variations in Overland Flows

Willi H. Hager

École Polytechnique Fédérale de Lausanne,
Switzerland

The investigation analyses the effects of local bottom slope and roughness coefficient variations in overland flow over a plane by using the kinematic wave theory. Results are compared with the usual approach, and it is found that certain configurations of surface topography and roughness characteristics yield results, that deviate from the usual predictions.

Introduction

Overland flows are the result of complex interactions regarding precipitation, infiltration, evaporation and storage effects. A complete mathematical description of flow phenomena is possible in principle, but will be extremely time-consuming and sophisticated with respect to the numerical treatment. A simpler approach assumes one-dimensional flow characteristics, for which de Saint-Venant's equations hold. Yet, the solution procedure is far from being elementary, and a proper numerical treatment must include shock wave analysis, among other pecularities (Abbott 1966).

Since typical Froude numbers F *and* relative flow depths are small when compared to unity, the *kinematic wave theory* described extensively by (Eagleson 1970) allows an effective and accurate modelling of the main flow properties. This

principle reason makes the kinematic wave approach so widely applied in hydrology. The successful investigations of (Wooding 1965) and (Woolhiser and Liggett 1967) consider the simplest catchment area, consisting of a plane with constant bottom slope and constant roughness characteristics. Solutions for the resulting discharge as a function of space and time may be computed analytically, provided the excess rainfall remains essentially constant. Note, however, that the effect of locally variable bottom geometry and roughness coefficient on the resulting hydrographs have not yet been analysed in detail. The usual approach assumes more or less constant values of bottom slope and roughness coefficient along a reach, without accounting for the complex basin topology. The present study aims at investigating these effects in general by assuming plausible relations for the two parameters in question. Analysis will be restricted to the usual assumption of constant excess rainfall, and comparisons include the rising hydrograph and resulting peak discharge.

The results of the present investigation are of particular importance regarding the *simplicity of the kinematic wave approach.* The non-dimensional representation of solutions allows a simple and direct application to realistic cases. Further, it will be possible to compare results of the present study with the well-known results valid for catchment areas with constant bottom slope and constant roughness coefficient.

Governing Equations

Flows with predominant direction may be modelled using the (one-dimensional) de Saint-Venant equations. Typical overland flow properties are:

- Low Froude number;
- Low flow depth when compared to the elevation difference of two points of the reach.

These properties allow the simplified version to be valid (Eagleson 1970), namely the kinematic wave equations

$$\frac{\partial h}{\partial t} + \frac{\partial q}{\partial x} = p \quad , \tag{1}$$

$$S_0 - S_f = 0 \tag{2}$$

in which Eq. (1) corresponds to the full continuity relation for plane flows, while Eq. (2) is the simplified version of the dynamical relation. The latter states that friction slope S_f is balanced by the bottom slope S_0, the resulting flows are said to be pseudo-uniform. Eq. (1) relates flow depth h and discharge q per unit width with precipitation p. Note that x and t are the longitudinal coordinate and time, respectively.

For relatively *heavy* precipitation p, flow state will be turbulent; friction slope then may be adequately expressed by the Manning-Strickler formula

$$S_f = \frac{q^2}{K^2 h^{10/3}} \qquad (3)$$

in which $K=1/n$ is the roughness coefficient having the order of $K \simeq 10^1$ for typical overland flow.

A) Effect of Local Bottom Slope Variation

Bottom Slope Function

The effect of the local bottom slope on the overland flow characteristics may be analysed by considering two typical points of the catchment area, namely its highest (top of the mountain) and lowest (lateral inflow to small stream) points. The average slope then obtains $i=z/L$ in which z is elevation difference and L length of the considered reach. Let $X=x/L$ be the non-dimensional longitudinal coordinate measured downwards from the highest point of the plane catchment area, then $X=0$ and $X=1$ correspond to the two points considered (see Fig. 1).

The effect of variable bottom geometry may be analysed by altering the shape of the curve connecting the two boundary points. A plausible approach is to consider bottom geometries of parabolic shape, for which

$$Z = 1 - (1+\mu)X + \mu X^2 \quad , \qquad (4)$$

$$X = \frac{x}{L} \quad , \qquad Z = \frac{z}{iL} \qquad (5)$$

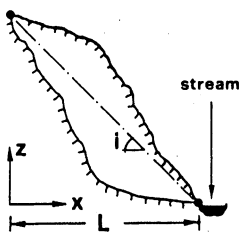

Fig. 1. Typical bottom geometry of catchment area with top of the mountain ($x=0$) and stream ($x=L$).

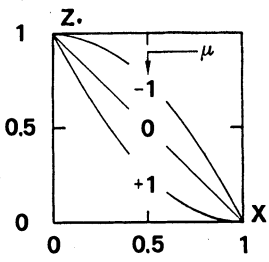

Fig. 2. Analytical approximation of the bottom geometry function $Z(X)$; $\mu=0$ corresponds to a bottom with constant slope, while $\mu=-1$ and $\mu=+1$ are the two extrema for which the bottom slope remain always positive.

Since $S_f \geq 0$ according to Eq. (3), S_0 must also be positive according to Eq. (2). Therefore, the possible domain of shape parameters μ is $-1 \leq \mu \leq +1$, and it is noted that $\mu=-1$ yields a horizontal bottom at $X=0$ (mountain peak), while this occurs at the catchment outlet $X=1$ for $\mu=+1$. Furthermore, the usual approach of a constant bottom slope results for $\mu=0$.

Since $S_0=-dz/dx=-i\, dZ/dX$, Eq. (4) yields for

$$S_0 = i[(1+\mu)-2\mu X] \tag{6}$$

Modified Flow Equation

Runoff from a catchment area may be predicted once the bottom geometry $S_0=S_0(x)$, the roughness coefficient $K=K(x)$, precipitation $p=p(x,t)$ are given and appropriate initial and boundary conditions are imposed. The simplest treatment assumes excess precipitation given as

$$\begin{aligned} p &= 0 \quad , \quad t < 0 \quad , \quad t > t_p \\ p &= p^* \quad , \quad 0 \leq t \leq t_p \end{aligned} \tag{7}$$

in which t_p is the time interval of constant precipitation p^*, and roughness coefficient as independent of x.

Combining Eqs. (2) and (3) yields the discharge-stage relation

$$q = K\sqrt{S_0}\, h^{5/3} \tag{8}$$

or, when accounting for the bottom geometry function Eq. (6)

$$q = K\sqrt{i}\,[(1+\mu)-2\mu X]^{1/2}\, h^{5/3} \tag{9}$$

The scalings

$$\begin{aligned} X &= \frac{x}{L} \quad , \quad T = \frac{p^{*2/5}\, K^{3/5}\, i^{3/10}}{L^{3/5}} \quad , \\ Y &= \left(\frac{K i^{1/2}}{p^* L}\right)^{3/5} h \quad , \quad Q = \frac{q}{p^* L} \end{aligned} \tag{10}$$

transform Eqs. (1) and (9) into

$$\frac{\partial Y}{\partial T} + \frac{\partial Q}{\partial X} = 1 \quad , \tag{11}$$

$$Q = (1+\mu-2\mu X)^{1/2}\, Y^{5/3} \tag{12}$$

or, since μ is independent of time and space

$$\frac{\partial Q}{\partial X} = \frac{-\mu Y^{5/3}}{(1+\mu-2\mu X)^{1/2}} + \frac{5}{3}(1+\mu-2\mu X)^{1/2} Y^{2/3} \frac{\partial Y}{\partial X} \tag{13}$$

from Eq. (12). Finally, upon inserting this into Eq. (11), the governing equation becomes

$$\frac{\partial Y}{\partial T} + \frac{5}{3}(1+\mu-2\mu X)^{1/2} Y^{2/3} \frac{\partial Y}{\partial X} = 1 + \frac{\mu Y^{5/3}}{(1+\mu-2\mu X)^{1/2}} \qquad (14)$$

which is a first order, non-linear partial differential equation for the unknown $Y(X,T)$ subject to the conditions $Y(0,T)=0$ (no flow on top of mountain) and $Y(X,0)=0$ (initially dry catchment area). Note that this reduces for *constant bottom slope* ($\mu=0$) to (see e.g. Eagleson 1970)

$$\frac{\partial Y}{\partial T} + \frac{5}{3} Y^{2/3} \frac{\partial Y}{\partial X} = 1 \qquad (15)$$

Solution

The characteristic form of Eq. (14) is (see e.g. Abbott 1966)

$$dT = \frac{3dX}{5(1+\mu-2\mu X)^{1/2} Y^{2/3}} = \frac{dY}{1 + \frac{\mu Y^{5/3}}{(1+\mu-2\mu X)^{1/2}}} \qquad (16)$$

Note that time T misses explicitely in this system. The solution of the equation formed by the center and right hand-sides obtains (see Appendix I)

$$Y = \left[\frac{(1+\mu-2\mu X)^{1/2}}{-2\mu} + \frac{C}{(1+\mu-2\mu X)^{1/2}}\right]^{3/5} \qquad (17)$$

in which C is the constant of integration. The particular case $Y(0)=0$ yields

$$Y^0 = \left[\frac{X}{(1+\mu-2\mu X)^{1/2}}\right]^{3/5} \qquad (18)$$

and corresponds to the *steady state flow profile* $Y=Y(X)$ represented graphically in Fig. 3 for typical values of μ. It is noted that all curves intersect at points (0,0) (as imposed) and (0.5, 0.66). In the interval $0 \leq X < 0.5$, the curve with $\mu=-1$ lies above all others, while this is the lowest curve for $0.5 < X \leq 1$. Because the bottom slope vanishes for $\mu=1$ at $X=1$, corresponding flow depth Y tends to infinity.

The general solution of Eq. (17) is obtained by setting $Y(X=X_0)=0$, whence

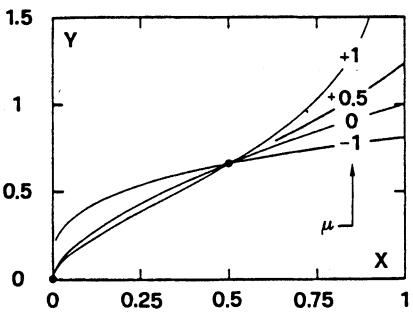

Fig. 3. Steady state surface profiles $Y(X)$ for various typical bottom geometry parameters μ.

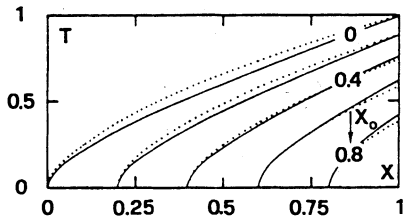

Fig. 4. Time-space locii on which Eq. (19) is valid. Note that $\mu=+0.5$ (solid curves) and $\mu=0$ (dotted curves).

$$Y(X) = \left[\frac{X-X_0}{(1+\mu-2\mu X)^{1/2}} \right]^{3/5} \qquad (19)$$

in which X_0 designates the constant of integration for this equation. The time-space coordinates on which Eq. (19) is valid are evaluated with the relation given by the first and second terms of Eq. (16). Eliminating $Y(X)$ with Eq. (19) then yields

$$dT = \frac{3dX/5}{(1+\mu-2\mu X)^{3/10}(X-X_0)^{2/5}} \qquad (20)$$

subject to the condition $T(X=X_0)=0$. This has been solved numerically, and typical solutions are plotted in Fig. 4. Combining this with Eq. (19), the complete solution $Y=Y(X,T)$ is found. Fig 5 represents the result for the particular values $\mu=\pm 0.5$, and it is observed that, for a specific location X, $Y(T)$ increases steadily whenever $0\leq X\leq X_c$, but then remains constant for any time $T>T_c$, T_c being the time of concentration. The coordinates (X_c, T_c)are determined by Eq. (20) by

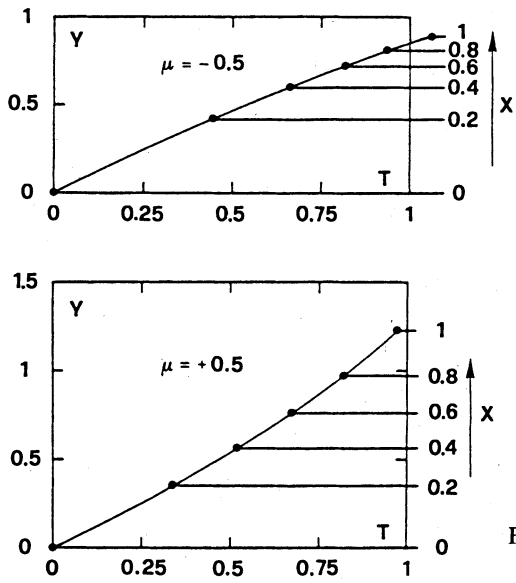

Fig. 5. Hydrographs $Y(X,T)$ for $\mu=-0.5$ (top) and $\mu=+0.5$ (bottom).

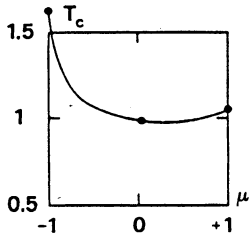

Fig. 6. Time of concentration T_c as a function of bottom shape parameter μ.

setting $X_0=0$. An evaluation of the integral

$$T_c = \int_0^1 \frac{3dX/5}{(1+\mu-2\mu X)^{1/2}\, X^{2/5}} \qquad (21)$$

is shown in Fig. 6 as $T_c(\mu)$ (for details see Appendix II). For fixed μ the plot divides values of time T into two ranges, namely $T<T_c$ and $T>T_c$; the first case applies to flows which have not yet reached steady flow conditions, whereas the second refers to times with steady flow conditions (see also Eagleson 1970, or Overton and Meadows 1976). This state is reached whenever precipitation time t_p is larger than the corresponding time of concentration.

Discussion of Results

Preceding analysis indicates that both, time of concentration T_c *and* maximum flow depth Y_{max} depend on the bottom shape parameter μ. If $T_p \geq T_c$ at a particular location X, steady flow characteristics occur, and discharge becomes the maximum value, $Q=Q_{max}$. The non-dimensional discharge-flow depth relation Eq. (12), combined with Eq. (19), may be written as

$$Q(X) = X - X_0 \qquad (22)$$

Maximum discharge appears for $X_0=0$, whence $Q_{max}=X$ or, since $0 \leq X \leq 1$, $Q_{max,abs}=1$ independent of μ. Consequently, the effect of variable bottom geometry vanishes for *steady flow conditions* with respect to the maximum possible discharge.

Fig. 7 shows the rising part of the surface profiles $Y(T)$, and corresponding maximum reach $X=1$ is denoted by a spot. It is observed that, for a particular time T, flow depth is highest in the case $\mu=+1$ (flat downstream portion) and lowest for $\mu=-1$. Peak discharge occurs after relatively short time for $\mu=+1$ ($T_c \simeq 0.93$), while it takes $T_c \simeq 1.62$ for $\mu=-1$; note that corresponding time is $T_c=1$ for $\mu=0$ as given by Eagleson (1970).

The non-steady development of discharge Q as a function of time T is evaluated with the aid of Eqs. (21) and (22), the result being

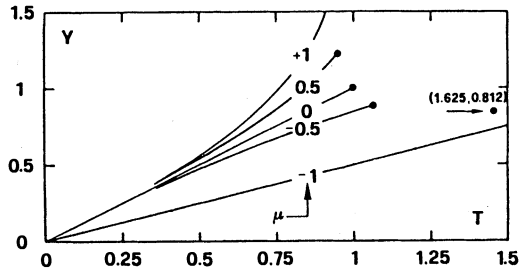

Fig. 7. Flow profiles $Y(T)$ at location $X=1$ (rising portion of hydrograph) for various typical values of μ. Dots indicate the transition between unsteady and steady flow characteristics, and corresponding time is time of concentration T_c.

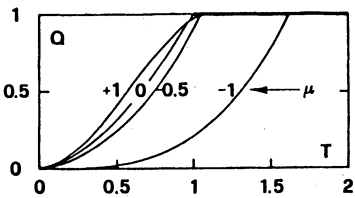

Fig. 8. Rising portion of hydrograph $Q(T)$ at lowest point of catchment area $X=1$ for various significant bottom shape parameters μ. Note that transition between unsteady and steady flows appears as soon as $Q=1$.

$$T = \int_0^Q \frac{3dQ/5}{(1+\mu-2\mu Q)^{3/10} Q^{2/5}} \qquad (23)$$

This is plotted in Fig. 8 as $Q(T)$ and refers to the maximum downstream length $X=1$. Note that hydrographs deviate only slightly from the usual approach ($\mu=0$), provided $-0.5 \leq \mu \leq +1$. However, differences become significant whenever $\mu \rightarrow -1$. Since the usual valley shape is rather between $0 \leq \mu \leq +1$ (see Fig. 2), the effect of μ on the resulting hydrograph is normally insignificant. To the lowest order of approximation hydrological computations may be evaluated assuming the averaged bottom slope instead of accounting for the complete bottom topography. This important conclusion allows a simplified description of complicated basins and is particularly well-suited for the kinematic wave approximation. Note, however, the limitations of the above statements regarding valley shapes with $\mu \rightarrow -1$ and predictions regarding the surface profiles (see Fig. 3).

The above analysis assumes constant precipitation. It is possible to extend considerations for time-dependent precipitations, $p=p(t)$, by using an appropriate hydrological model (see e.g. Hager 1984). Typical evaluations suggest analogous conclusions as have been found above.

B) Effect of Local Roughness variation

Roughness Coefficient Distribution

The roughness coefficient is in general a function of time *and* space; for a strip with unit width it may be expressed as $K=K(x,t)$. Note that this coefficient is a typical *macroscopic* quantity difficult to define for a particular reach of the basin. Moreover, investigations concerning *strictly* uniform flow conditions in channels with well-defined boundaries are still in vital research stage (Hager 1984). Owing to these difficulties, $K=1/n$ in overland flows is a quantity to be *estimated*. Note that, for fixed flow depth and fixed bottom slope, discharge augments linearly with K; this latter parameter influences significantly the final result, therefore.

The kinematic wave approximation is a macroscopic approach; unevenness in both K and S_0 with respect to the longitudinal coordinate (and to time) are usually ignored, and both are considered as essentially independent from x and t. Typical valley shapes reveal that K is higher at the top zone of it than at the lowlands. This general trend results from relative smooth surface at the upper valley regions, and from cultivated planes at the lower ones. Evidently, these tendencies may also be inverse, but, for a sensitivity analysis, it seems appropriate to vary $K=K(x)$ linearly with the longitudinal coordinate. Ensuing considerations are the counterpart of the above. Henceforth bottom slope S_0 will be assumed constant, $S_0=i$, while the effect of local roughness variation will be investigated, thereby accounting for Eq. (7) regarding the precipitation characteristics.

Let K_a be the average roughness coefficient for turbulent flow, then

$$K(X) = K_a[1+\phi(2X-1)] \tag{24}$$

corresponds to a linear variation of local roughness coefficient K. This relation is shown graphically in Fig. 9, and it is noted that the distribution factor ϕ is physically defined in the domain $-1\leq\phi\leq+1$. Inserting Eq. (24) into Eq. (8) results in

$$q = K_a[1+\phi(2X-1)]\sqrt{i}\,h^{5/3} \tag{25}$$

or, upon introducing the scalings Eq. (10)

$$Q = [1+\phi(2X-1)]Y^{5/3} \tag{26}$$

Combining this with the non-dimensional continuity Eq. (11) leads to the analogon of relation Eq. (14), namely

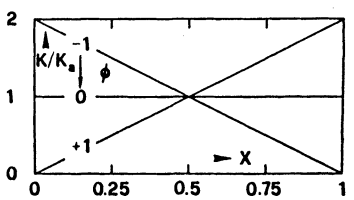

Fig. 9.
Assumed local distribution of roughness coefficient $K(X)/K_a$. The kinematic wave theory applies only for $-1\leq\phi\leq+1$.

$$\frac{\partial Y}{\partial T} + \frac{5}{3}\left[1+\phi(2X-1)\right]Y^{2/3}\frac{\partial T}{\partial X} = 1 - 2\phi Y^{5/3} \qquad (27)$$

which must be solved subject to the conditions $Y(T=0)=Y(X=0)=0$ as above. Note, that the particular and well-analysed case defined by Eq. (15) occurs for $\phi=0$.

Solution

The equivalent characteristic system to Eq. (27) reads

$$dT = \frac{3\,dX/5}{\left[1+\phi(2X-1)\right]Y^{2/3}} = \frac{dY}{1-2\phi Y^{5/3}} \qquad (28)$$

Again the steady state solution is described by the center and right hand-side parts and reads (see Appendix III)

$$Y(X) = \left[\frac{X}{1+\phi(2X-1)}\right]^{3/5} \qquad (29)$$

on which $Y(X=0)=0$ has been imposed. This is plotted in Fig. 10, and it may be noted that point (0.5, 0.66) is commom to all curves. Moreover, all curves except that for $\phi=+1$ start in the origin, while the last remains independent of X (real uniform flow with depth $Y=0.5^{3/5}\simeq 0.66$); the curve with $\phi=-1$ tends to infinity for $X\rightarrow 1$.

Discharge $Q(X)$ for *steady flow conditions* may directly be computed combining Eqs. (26) and (29), the result being

$$Q(X) = X \qquad (30)$$

which is independent of ϕ and comparable to Eq. (22).

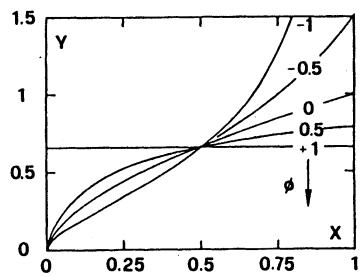

Fig. 10. Surface profiles $Y(X)$ for steady flow conditions ($T>T_c$) and for various roughness coefficient parameters ϕ.

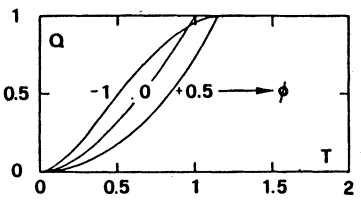

Fig. 11. Effect of ϕ on rising portion of hydrograph $Q(T)$ at location $X=1$ (stream inflow).

The time-space locii leaving at point (0,0) are prescribed by the first and center terms of Eq. (28), which, upon eliminating $Y(X)$ with Eq. (29) obtains

$$dT = \frac{3dX/5}{[1+\phi(2X-1)]^{3/5}\, Y^{2/5}} \qquad (31)$$

This has been solved numerically using the expression derived in Appendix IV for its initialisation. The result, $T=T(X)$, allows determination of the *unsteady portion* of the solution, and typical results are plotted in Fig. 11. Note again that, for $-1 \leq \phi \leq 0.5$, the effect of ϕ on $Q(T)$ is insignificant, but becomes important for $\phi \rightarrow +1$. This case, which corresponds to a catchment area being much rougher at the top zone than at the lowlands is seldom encountered in practise, yet it may reflect a realistic case. Conclusions regarding the local variation of bottom slope and roughness coefficient for both steady and non-steady flow phenomena thus resemble. To the lowest order of approximation, the roughness characteristics of a catchment area may be described using a properly chosen average value. Since this quantity is normally subject to considerable variation (estimation of upper and lower extrema), computations should preferably be performed for different *average* roughness coefficients, provided the local variation of $K(x)$ is not near the particular value $\phi=+1$.

Conclusions

This investigation analyses the effects of *local* bottom slope and roughness coefficient variations in overland flow by using the kinematic wave theory. The two respective parameters, μ and ϕ, are defined in the limits -1 to + 1, and $\mu=\phi=0$ reflects the usual approach accounting for an average bottom slope and friction coefficient along the reach.

It is found that the effect of μ and ϕ is significant on the resulting surface profile but may be ignored regarding the discharge characteristics, provided valleys are not flat in the upper and steep in the lower zones. In addition, the local effect of roughness coefficient must be accounted for when surfaces are significantly rougher at the upper than at the lower zones of the catchment area.

The present investigation allows a simple application of results since all computations are performed with non-dimensional quantities. This particular notation allows a thorough comparison between different configurations of bottom and roughness coefficient variations.

References

Abbott, M. B. (1966) *Method of Characteristics.* American Elsevier, New York.

Eagleson, P. S. (1970) *Dynamic Hydrology.* McGraw-Hill Book Company, New York.

Hager, W. H. (1984) A simplified hydrological rainfall-runoff model. *J. Hydrology,* to be published.

Hager, W. H. (1984) Abflusseigenschaften in offenen Kanaelen. Schweizer Ingenieur und Architekt SIA, to be published.

Overton, D. E., and Meadows, M. E. (1976) *Stormwater Modelling.* Academic Press, New York, N.Y., 1976.

Wooding, R. A. (1965) A hydraulic model for the catchment-stream problem. *J. Hydrology, Vol. 3,* pp. 254-267.

Woolhiser, D. A., and Liggett, J. A. (1967) Unsteady one-dimensional flow over a plane-The rising hydrograph. *Water Res.Res., Vol. 3,* pp. 753-771.

Notations

The following symbols have been used in this paper:

h (m)	flow depth	t (s)	time
i (–)	average bottom slope	t_c (s)	time of concentration
S_f (–)	friction slope	t_p (s)	time of precipitation
S_o (–)	bottom slope	x (m)	longitudinal coordinate
$K(m^{1/3}s^{-1})$	roughness coefficient	X (–)	non-dimensional coordinate x
L (m)	length of catchment area	Y (–)	non-dimensional flow depth
$p(ms^{-1})$	precipitation	z (m)	elevation
$p^*(ms^{-1})$	average precipitation	Z (–)	non-dimensional elevation
$q(m^2s^{-1})$	discharge per unit width	μ (–)	bottom slope parameter
Q (–)	non-dimensional discharge	ϕ (–)	roughness coefficient parameter

Appendix I – Solution of Eq. (16)

The differential equation consisting of the center and the right hand side part of Eq. (16) is

$$\frac{dX}{(1+\mu-2\mu X)^{1/2}}\left(1+\frac{\mu Y^{5/3}}{(1+\mu-2\mu X)^{1/2}}\right)=\frac{5}{3}Y^{2/3}\,dY \qquad (32)$$

With the substitutions

$$W^2=1+\mu-2\mu X \quad , \quad V^3=Y \qquad (33)$$

this transforms into

$$-\frac{dW}{5}\left(\frac{1}{\mu V^4}+\frac{V}{W}\right)=dV \qquad (34)$$

which is a differential equation of the Bernoulli type. Upon introducing the new variable $U=V^5$, one has

$$-dU = \left(\frac{1}{\mu} + \frac{U}{W}\right) dW \tag{35}$$

The solution of the homogeneous equation is $U=\bar{C}/W$, in which $\bar{C}$ is the constant of integration to be varied for the solution of the non-homogeneous differential equation. The final solution is computed straightforward, the result being

$$U = \frac{-W}{2\mu} + \frac{C}{W} \tag{36}$$

with C as the real constant of integration. Resubstitution of U and V yields

$$Y = \left(\frac{-W}{2\mu} + \frac{C}{W}\right)^{3/5} \tag{37}$$

in which W is given by Eq. (33).

Appendix II – Solution of Eq. (20) for $X \rightarrow 0$

The integral given in Eq. (19) cannot be solved generally by analytical means; its numerical evaluation leads to difficulties for $X \rightarrow 0$, since $X=0$ corresponds to a singularity. In order to initiate the integration procedure, an analytical solution must be found for $X \rightarrow 0$. Excluding the case where $\mu=-1$ (which is treated below), one has instead of Eq. (20) for $X \rightarrow 0$

$$T_c = \int_0^1 \frac{3\,dX/5}{(1+\mu)^{3/10}\left(1-\frac{2\mu X}{1+\mu}\right)^{3/10} X^{2/5}} \tag{38}$$

or, when developing term $\{1-(2\mu X)/(1+\mu)\}^{3/10}$ in a Taylor series and retaining only the first order correction term

$$T_c = \frac{3/5}{(1+\mu)^{3/10}} \int_0^{X_c^*} \frac{\left(1+\frac{3\mu X}{5(1+\mu)}\right) dX}{X^{2/5}} + \int_{X_c^*}^1 \frac{3\,dX/5}{(1+\mu-2\mu X)^{3/10} X^{2/5}} \tag{39}$$

in which $X_c^* << 1$. The first of these integrals will be used subsequently and is denoted as I_1. Its evaluation is straightforward, the result being

$$I_1 = \frac{X_c^{3/5}}{(1+\mu)^{3/10}}\left(1+\frac{9\,\mu X_c}{40(1+\mu)}\right) \tag{40}$$

This has been used for $X_c=0.01$, and the numerical evaluation of the second integral in Eq. (39) finally allows Fig. 5 to be drawn. Eq. (20) may be solved analytically for the cases in which $\mu=0$, resulting in

$$T_c = X_c^{3/5} \tag{41}$$

and $\mu=-1$, for which

$$T_c = (2^7 X_c^3)^{1/10} \tag{42}$$

Appendix III – Solution of Eq. (28), steady state conditions

The center and the right hand sides of Eq. (28) define the steady-state portion of the complete solution. With

$$\bar{W} = 1 + \phi(2X-1) \quad , \quad \bar{V}^3 = Y \tag{43}$$

it transforms to

$$\frac{d\bar{W}}{10\phi\bar{W}} \left(\frac{1}{\bar{V}^4} - 2\phi\bar{V} \right) = d\bar{V} \tag{44}$$

which is of Bernoulli type. With $\bar{U}=\bar{V}^5$, one has the linear equation

$$\frac{d\bar{W}}{2\phi\bar{W}} \left(1 - 2\phi\bar{U} \right) = d\bar{U} \tag{45}$$

of which the solution reads

$$\bar{U} = \frac{1}{2\phi} + \frac{C}{\bar{W}} \tag{46}$$

with C as constant of integration. Accounting for the boundary condition $Y(X=0)=0$, the final result obtains after resubstituting

$$Y(X) = \left[\frac{X}{1+\phi(2X-1)} \right]^{3/5} \tag{47}$$

Appendix IV – Solution of Eq. (31) for $X \to 0$

Eq. (31) describes the time-space coordinates on which Eq. (29) is valid. It reads

$$dT = \frac{3\,dX/5}{[1+\phi(2X-1)]^{3/5}\,X^{2/5}} \tag{48}$$

Excluding the particular value $\phi=1$, this may equally be written for $X \to 0$ as

$$dT = \frac{3\,dX/5}{(1-\phi)^{3/5}\left[1+\frac{2\phi X}{1-\phi}\right]^{3/5} X^{2/5}} \simeq \frac{\frac{3}{5}\left(1-\frac{6\phi X/5}{1-\phi}\right)dX}{(1-\phi)^{3/5}\,X^{2/5}} \tag{49}$$

Integration of this is straightforward, the result being

$$T = \left(\frac{X}{1-\phi} \right)^{3/5} \left(1 - \frac{9\,\phi X}{20(1-\phi)} \right) \quad , \quad X \to 0 \tag{50}$$

The values $\phi=0$ and $\phi=1$ are special, since a complete analytical integration is possible. The respective solutions become

$$T_c = X_c^{3/5} \quad , \quad \phi = 0 \tag{51}$$

and

$$T_c = \frac{3}{5 \times 5^{3/5}} \ln(X_c) + C \quad , \quad \phi = +1 \tag{52}$$

with C as constant of integration. Since $\ln(X_c) \to -\infty$ for $X_c \to 0$, it is impossible to define C. The solution thus has been found approximately by starting with $T_c(X_c=0.001)=0$.

Received: 23 July, 1984

Adress: École Polytechnique Fédérale de Lausanne,
Départment de Génie Civil,
Institut de Travaux hydrauliques, CCH,
CH-1015 Lausanne,
Switzerland.